Gate-Tunable Spin-Orbit Coupling in a Germanium Hole Double Quantum Dot

He Liu,[1,2,‡] Ting Zhang,[1,2,‡] Ke Wang,[1,2,‡] Fei Gao,[3] Gang Xu,[1,2] Xin Zhang,[1,2] Shu-Xiao Li,[1,2]
Gang Cao,[1,2] Ting Wang,[3] Jianjun Zhang,[3] Xuedong Hu,[4] Hai-Ou Li,[1,2,*] and Guo-Ping Guo[1,2,5,†]

[1] *CAS Key Laboratory of Quantum Information, University of Science and Technology of China, Hefei, Anhui 230026, China*
[2] *CAS Center for Excellence and Synergetic Innovation Center in Quantum Information and Quantum Physics, University of Science and Technology of China, Hefei, Anhui 230026, China*
[3] *Institute of Physics and CAS Center for Excellence in Topological Quantum Computation, Chinese Academy of Sciences, Beijing 100190, China*
[4] *Department of Physics, University at Buffalo, SUNY, Buffalo, New York 14260, USA*
[5] *Origin Quantum Computing Company Limited, Hefei, Anhui 230026, China*

Hole spins confined in semiconductor quantum dot systems have gained considerable interest for their strong spin-orbit interactions (SOIs) and relatively weak hyperfine interactions. Here, we experimentally demonstrate a tunable SOI in a double quantum dot in a germanium (Ge) hut wire (HW), which could help to enable fast all-electric spin manipulations while suppressing unwanted decoherence. Specifically, we measure the transport spectra in the Pauli-spin-blockade regime in the double-quantum-dot device. By adjusting the interdot tunnel coupling, we obtain an electric-field-tuned spin-orbit length of $l_{\text{SO}} = 2.0\text{--}48.9$ nm. This tunability of the SOI could pave the way toward the realization of high-fidelity qubits in Ge HW systems.

I. INTRODUCTION

Hole-spin qubits in Ge quantum dots (QDs) are intriguingly attractive in quantum-information processing because of their advantageous properties [1–8]. Compared with the III-V materials, natural Ge—a group-IV semiconductor—contains a much lower abundance of nuclear-spin isotopes and can be further purified to become a nuclear-spin-free host, greatly improving the coherence times of spin qubits [9,10]. Furthermore, because the hole states are formed of p-atomic-orbital wave functions, the contact hyperfine interaction (HFI) vanishes completely, and the anisotropic HFI (dipole-dipole and angular momentum terms) dominates [11]; the latter can be reduced or even eliminated by motional averaging [12–15]. Another significant advantage of hole spins over electron spins is their much stronger spin-orbit interaction (SOI) [16], which allows an all-electrical manipulation of single hole spins [1–8,17–20] and simplifies device fabrication. As a material platform, Ge hut wires (HWs) [21] are considered a strong contender for large-scale quantum circuits because of some favorable properties. For example, the

direct Rashba SOI (DRSOI) [22,23] in one-dimensional hole nanowires has yielded the fastest Rabi frequency to date [3], and the realization of site-controlled Ge HWs [24] could benefit the scaling up of spin-qubit applications.

The main challenge faced by a hole-spin-based quantum computer lies in the extremely strong DRSOI in Ge HWs. On one hand, it is the crucial ingredient that allows ultrafast qubit operations. On the other hand, it enables undesirable decoherence by allowing strong coupling to all electrical fluctuations in the environment, such as phonons and charge noise [25–32]. To benefit from the DRSOI while overcoming its drawbacks, one can take advantage of the fact that the DRSOI is highly tunable with electric fields [22,23]. One can thus realize different features (e.g., fast operation speeds and long coherence times) in different SOI strengths that are adjusted by gate voltages [33]. Such tunability has indeed been explored recently in experiments demonstrating a spin-orbit switch in a core-shell Si-Ge nanowire [2].

One interesting feature of the Ge HW system is the variety of SOIs it has. In addition to the DRSOI, other SOI mechanisms, such as an interface SOI and an intrinsic SOI, may also be present and important [34,35]. In particular, by applying a certain electric field, we may be able to completely turn off the total SOI at an operating sweet spot for the qubits (idle state), where the effects of charge noise and phonons are strongly suppressed [34]. This electrical

---

*haiouli@ustc.edu.cn
†gpguo@ustc.edu.cn
‡H. Liu, T. Zhang, and K. Wang contributed equally to this work.

tunability of the SOI could also provide a means for precise control over the g factor, which can be exploited to address qubits individually in a large-scale array [33]. Therefore, a better understanding and control of the SOI in Ge HW QDs is of critical importance if longer relaxation and coherence times and higher-quality spin control are to be gained.

Here, we determine and study the main hole-spin relaxation mechanisms on a highly tunable double quantum dot (DQD) fabricated in a Ge HW. We measure the leakage current in the Pauli-spin-blockade (PSB) regime to probe the various relaxation processes in the DQD by varying the applied magnetic field and interdot detuning. By increasing the tunnel coupling within two dots, we find that the current peak is split into two peaks in a magnetic field. This transition is induced through the combined effects of the SOI and Zeeman splitting. Based on our numerical simulations [36], we extract a gate-tunable SOI strength with a spin-orbit length of $l_{SO} = 2.0$–48.9 nm, which provides clear evidence for a potential spin-orbit switch in a Ge HW DQD.

II. RESULTS AND DISCUSSION

A. Experimental setup

Our few-hole DQD device (see the Appendix for more details) is fabricated following established procedures by gating a Ge HW [Fig. 1(a)]. The self-assembled Ge HWs are grown on a Si(001) wafer by solid-source molecular beam epitaxy [21]. After wet etching with buffered hydrofluoric acid, two 30-nm-thick palladium contact pads with a gap of around 265 nm are formed by electron-beam evaporation. The sample is then covered with a 20-nm insulating layer of hafnium oxide to suppress gate leakage.

Finally, three 35-nm-wide top gates are fabricated with titanium and palladium (3 and 25 nm thick). We perform the measurements in a liquid He-3 refrigerator at a base temperature of 240 mK, with an out-of-plane magnetic field.

By applying positive voltages to three top gates to create the confinement potential, a DQD in series along the nanowire is formed between them [Fig. 1(c)]. In the Coulomb-blockade region, the number of hole occupations (m, n) in the left and right dots can be adjusted using gates L and R; gate C is used to adjust the tunnel coupling between the two dots. Figure 1(b) shows a typical charge-stability diagram of the DQD measured from the transport current with a source-drain bias of $V_{SD} = +2.5$ mV. With hole transport allowed only at triple points, we detect an array of bias triangles. Here, the green lines separating the different Coulomb-blockade regions indicate the change of hole occupations in the DQD, denoted by (m, n). From the slopes and spacings of the transition lines, we obtain values of the lever arms and charging energies for each QD (see the Appendix).

B. Pauli-spin blockade

The bias triangle in the red dashed circle in Fig. 1(b) exhibits PSB characteristics of particular interest to us [37–39]. PSB normally occurs in the transition from charge state $(2m + 1, 2n + 1)$ to $(2m, 2n + 2)$, which can be equivalently described as $(1,1)$ to $(0,2)$ for simplicity and thought of as a feature of the two-hole spectrum. When the DQD is in the $T(1,1)$ state [Fig. 2(a)], transport is blocked: the transition from $T(1,1)$ to $S(0,2)$ is forbidden by spin
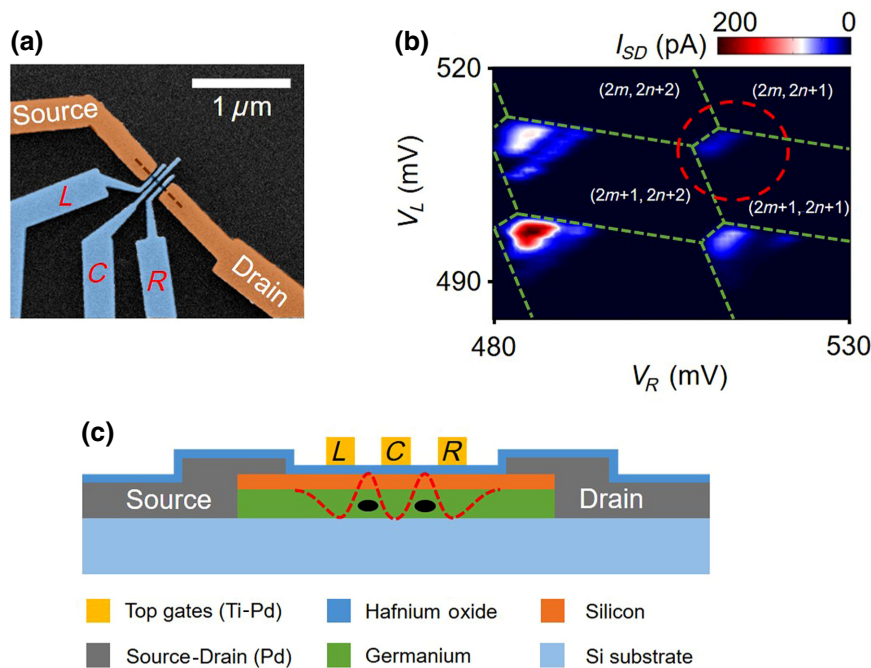
(a)

(b)

FIG. 1. (a) Scanning-electron-microscopy image of the hole DQD in a Ge HW. (b) Charge-stability diagram of the Ge DQD as a function of V_L and V_R with $V_{SD} = +2.5$ mV. Green dashed lines separate the charge states. Bias triangle in the encircled region is investigated in detail. (c) Schematic cross-section structure of the Ge HW DQD.

(c)

(a)

(b)

I_{SD} (pA)

(c)

I_{SD} (pA)
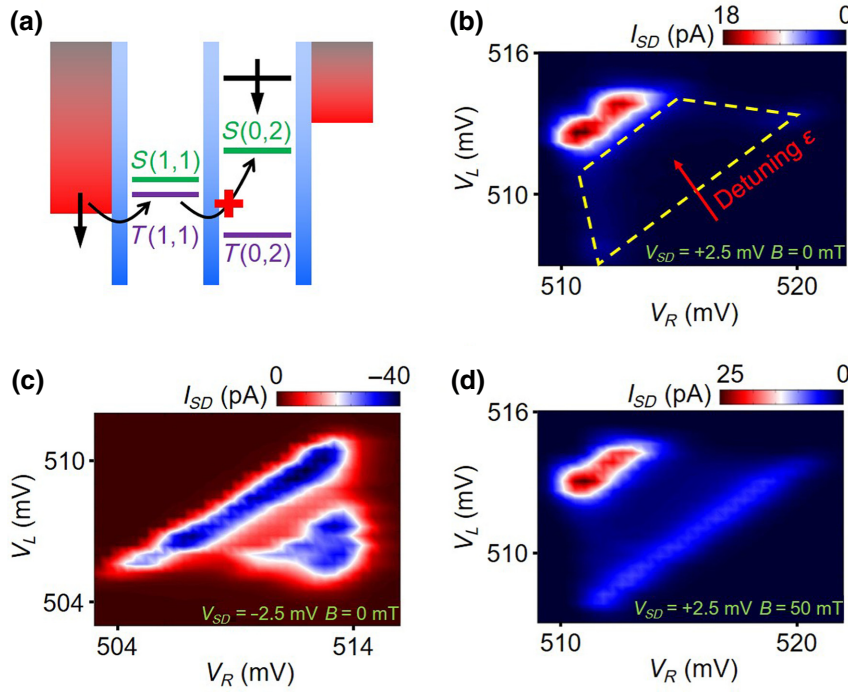
(d)

I_{SD} (pA)

FIG. 2. (a) Schematic diagram of the PSB for a hole DQD. (b) Bias triangle described in the main text exhibits the PSB signatures. Strong suppression of the current is observed in the region bounded by the dashed line. Detuning of the DQD is changed along the red arrow. (c) Reversing the bias, an enhancement of the leakage current is observed throughout the triangle. (d) At positive bias, a large leakage current appears at the base of the triangle with a 50-mT magnetic field due to the SOI. Here, the voltage of gate C is 596 mV.

conservation, while the energy of $T(0,2)$ is too high to access [37].

Figure 2(b) shows a magnification of the bias triangle marked in Fig. 1(b) by the red dashed circle. Because of PSB, we observe current rectification in the trapezoidal region indicated by the dashed line. We modify the detuning of the potentials of the left and right QDs by changing the voltages of gates L and R (red arrow). Once the energy levels of $T(1,1)$ and $T(0,2)$ align, the PSB is lifted and transport through the DQD is allowed, leading to an enhanced current at the top of the bias triangle. When we reverse the source-drain bias, a nonzero current is observed throughout the triangular region in Fig. 2(c) because the hole can transition freely from the $S(0,2)$ to the $S(1,1)$ state. In addition, after applying a 50-mT magnetic field, a large leakage current appears at the base of the triangle in Fig. 2(d), which is induced by the SOI, as we will elaborate next.

C. Transport spectra induced by the SOI

The PSB is lifted when a spin is flipped. Such a spin transition can occur via a variety of mechanisms: (i) the SOI can hybridize $T(1,1)$ with $S(0,2)$ via spin-flip tunneling [40,41]; (ii) the HFI can mix the different (1,1) states [42,43]; (iii) spin-flip cotunneling to the leads allows charge and spin exchange with the leads [44–47]; and (iv) the difference in g factors between the two dots couples $T_0(1,1)$ and $S(1,1)$ states [36], similar to the longitudinal Overhauser field, giving rise to a finite leakage current in the PSB region. To identify and study the main spin-relaxation mechanism(s) in our system, we measure the leakage-current spectra as a function of detuning and magnetic field with different interdot tunnel couplings in the bias triangle of Fig. 2(b). Varying the gate-C voltages can adjust the tunnel coupling between the two dots over a wide range, giving us a tuning knob to differentiate mechanism (i) from the others.

In the PSB regime, we find that the measured leakage-current spectra with relatively strong and weak interdot tunnel coupling [Figs. 3(a) and 3(b), respectively] show two completely different field-dependent behaviors. In the strong tunnel-coupling regime ($V_C = 596$ mV), the current spectrum shows a double-peak structure consisting of a dip at zero field and two current peaks at finite magnetic fields. This deep zero-field dip and the experimental temperature of 240 mK exclude the mechanism of spin-flip cotunneling, which leads to only a shallow dip for $k_B T \ll t$ [47]. Furthermore, spin mixing induced by the HFI is effective at a magnetic field of a few millitesla because of the weak HFI in Ge hole systems [11,48]. Therefore, the field dependence here can be well explained by a strong SOI and Zeeman splitting [see the energy-level diagrams in Figs. 3(c) and 3(d)]. At $B = 0$ mT, the tunnel coupling between the two dots couples $S(1,1)$ to $S(0,2)$ with coupling strength t, leading to strong hybridization and a large level anticrossing [Fig. 3(c)], while the three degenerate triplets $T(1,1)$ do not couple with $S(0,2)$ through spin-preserving tunneling and are energetically detuned from the singlet states, so that the effect of spin-flip tunneling is minimal. Furthermore, the large singlet anticrossing also limits hyperfine mixing between the (1,1) states, suppressing the leakage current at zero field [42]. However, at a finite magnetic field, the strong SOI in Ge
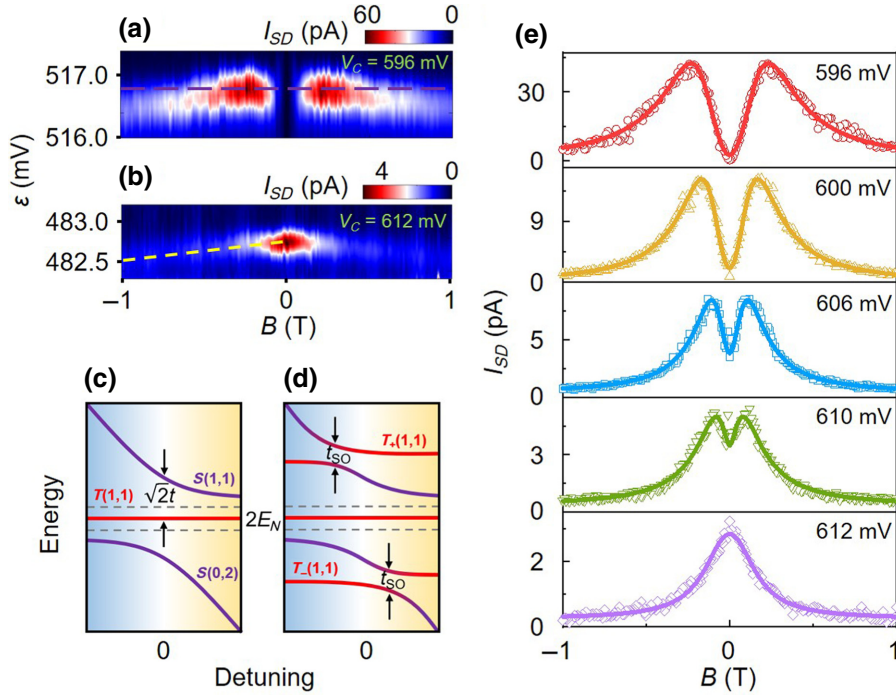
FIG. 3. (a),(b) Leakage-current spectra induced by the SOI with different tunnel couplings for magnetic fields in the range (−1 to 1 T). For large tunnel couplings in (a) ($V_C = 596$ mV), the spectrum shows a double-peak structure that consists of a dip at zero field and two current peaks at specific magnetic field strengths. For small tunnel coupling in (b) ($V_C = 612$ mV), the spectrum shows a single peak at zero magnetic field. (c),(d) Schematic energy-level diagrams for large tunnel couplings needed to explain the behavior of leakage current in Fig. 2(a). (e) Series of line cuts near zero detuning [as denoted by the purple dashed line in (a)] with different tunnel couplings. Increasing gate-*C* voltage from 596 to 612 mV decreases the coupling strength. Solid lines are fitted curves using the modified model of Ref. [36].

HWs hybridizes $T_{\pm}(1,1)$ and $S(0,2)$ with coupling strength t_{SO} [Fig. 3(d)], thereby increasing the leakage current. Given that the distance between current peaks induced by the SOI scales with strength t, in the weak tunnel-coupling regime ($V_C = 612$ mV), we observe only a single peak centered at zero field with a width of approximately 300 mT, which excludes any HFI effect [42,48]. In the strong tunnel-coupling regime, on the other hand, the large singlet anticrossing helps separate the two SOI-induced peaks in the leakage current, so that we can observe both of them experimentally. Using the slopes of the observed current lines [as denoted by the yellow dashed line in Fig. 3(b)], which can be interpreted as indicating resonances between $T_{-}(1,1)$ and $S(0,2)$, we obtain $g = 3.17$, which is in agreement with values obtained previously [49].

To better understand and quantitatively describe the observed transition, a series of line cuts [Fig. 3(e)] around zero detuning ($\varepsilon = 0$) are analyzed in the leakage-current spectra [as denoted by the purple dashed line in Fig. 3(a)] for different tunnel couplings. With decreasing tunnel coupling between the two dots, specifically, varying gate-*C* voltages from 596 to 612 mV, the magnetic field dependence of the leakage current induced by the SOI eventually transforms from a double-peak structure to a single peak. In this process, the magnitude of the leakage current and the distance between the two current peaks gradually decrease. Consequently, the dip at zero field finally disappears or is too narrow to be probed. In a high magnetic field, the energy level of $T_{-}(1,1)$ is pushed below $S(0,2)$ and drives the system into a Coulomb-blockade regime that suppresses the current. This SOI-induced behavior in

the leakage current that we observe is similar to that in Ge-Si core-shell nanowires, where it is measured in two different bias triangles [36]. Following Ref. [36], we apply the same modified model that considers the effects of both the SOI and the difference in g factors in the two dots to analyze leakage-current data.

D. Theoretical model and simulation

The bias triangle we study here is in the few-hole regime [3]. The Hamiltonian matrix of our effective two-hole system in the Pauli-blockade regime can then be presented on the triplet-singlet basis [$T_{+}(1,1)$, $T_{-}(1,1)$, $T_0(1,1)$, $S(1,1)$, $S(0,2)$] as [36]

$$H = \begin{pmatrix} E_Z & 0 & 0 & 0 & it_{+} \\ 0 & -E_Z & 0 & 0 & it_{-} \\ 0 & 0 & 0 & \xi B & 0 \\ 0 & 0 & \xi B & 0 & t \\ -it_{+} & -it_{-} & 0 & t & -\varepsilon \end{pmatrix}. \quad (1)$$

Here, E_Z describes the energy shift of polarized triplets with respect to the unpolarized triplet in a magnetic field. ε is the detuning between $S(1,1)$ and $S(0,2)$ states and is set to zero. t is the spin-preserving-tunneling matrix element between $S(1,1)$ and $S(0,2)$ states. t_{+} and t_{-} are the spin-flipping-tunneling matrix elements induced by the SOI from the two polarized triplets to $S(0,2)$, which satisfy the relationship $t_{+} = -t_{-} = t_{SO}$ due to time-reversal symmetry [41]. ξB describe the mixing between $T_0(1,1)$ and $S(1,1)$, which is caused by the difference of g factors in the two dots, with $\xi = (1/2)(g_L - g_R)/(g_L + g_R)$ [36,50]. The value of the effective g factor is expected to

be site dependent and depends on the microscopic characteristics of QDs, such as the confining potential [22,51], charge occupation [49], and the wave function [52]. We estimate that the value of ξ is around 0.14 from the electric dipole spin-resonance spectra of similar samples in Ge hut wires [3].

We diagonalize the above Hamiltonian and describe the dynamics of hole transport in our system with a master equation in the new basis:

$$\frac{d\rho}{dt} = -i[H^{\mathrm{diag}}, \rho] + \Gamma\rho + \Gamma_{\mathrm{rel}}\rho. \quad (2)$$

Here, ρ is the density matrix. Γ describes the hole transport between the DQD and leads, including decay to the drain lead and reloading from the source lead. Γ_{rel} describes the relaxation process from excited states to the ground state in the DQD. We obtain the density matrix of the steady state by solving the equation $d\rho/dt = 0$, and the current through the DQD can be expressed as $I = \sum_n p_n \Gamma|\langle n|\mathrm{S}(0,2)\rangle|^2$, where $p_n = \rho_{nn}$ and $|n\rangle$ refer to the eigenstates of the Hamiltonian in Eq. (1).

The theoretical model is particularly successful at reproducing the zero-detuning current traces [Fig. 3(e), solid lines] with parameters listed in Table I. Through the numerical simulation, we find that the magnitude of the leakage current is directly related to the tunneling rate between the DQD and the lead, Γ, and the relaxation rate, Γ_{rel}, directly determines the depth of the dip (i.e., the value of current at zero field). The tunneling rates within two dots (t and t_{SO}) cannot be determined independently and are related to the specific shape of the current curve.

E. Tunability of the SOI

Given the results of model parameters t and t_{SO} (see Table I), we extract a spin-orbit length of $l_{\mathrm{SO}} = 2.0 - -48.9$ nm from $t_{\mathrm{SO}}/t = (4/3)(l_{\mathrm{dot}}/l_{\mathrm{SO}})$ [53,54] and a dot-to-dot distance, l_{dot}, of about 75 nm. ξ, the relative g-factor difference between the two dots, is an assumed parameter in the calculation of l_{SO}. During the fitting process,

we find that, when the value of ξ varies within a certain range, the fitted value of t_{SO}/t hardly changes, which gives us confidence that the calculated value of l_{SO} should be reliable.

Here, the distance between two dots remains almost unchanged when adjusting the voltage of gate C with the same hole occupation, which we verify via simulation with COMSOL. This provides direct evidence that the spin-orbit length in our system can be highly tunable by changing the gate-C voltage [Fig. 4(a)]. A smaller l_{SO} at higher gate voltages is reasonable and is consistent with the known relationship between the direct Rashba coefficient and the average electric field tunable by the gate voltage [22,23]. These remarkably short l_{SO} values we obtain indicate a strong DRSOI in our system, and the tunability of the spin-orbit length is consistent with the results obtained in Ge-Si core-shell nanowires [2]. To extend the tunable range of l_{SO} further, we would need to optimize the electrode design to decrease the strength of the electric field or directly reduce the gate-C voltage, according to the curve trend in Fig. 4(a), resulting in a weaker SOI.

The high degree of tunability of l_{SO} is the key to a spin-orbit switch, which can be used to enable fast Rabi oscillation with a strong SOI and ensure longer coherence times when decreasing SOI [3]. This switchable qubit-operation scheme breaks the trade-off between coherence and speed of control (i.e., Rabi frequency) and greatly improves the qubit fidelity theoretically, which is of critical importance for fault-tolerant quantum computing [55]. Considering the presence of the Dresselhaus SOI induced by the interface-inversion asymmetry in Ge HWs [35], a "sweet spot" of operation may be present when the total SOI is completely turned off, as shown in Fig. 4(b) [34]. Here, the effective spin-orbit fields caused by different SOI mechanisms (B_R and B_D) are represented by arrows of different colors. The red arrow indicates the total spin-orbit field and is quenched when B_R and B_D are equal in amplitude but opposite in direction (marked in red star), which can be realized by combining the two characteristic advantages in Ge HWs: (i) the tunability of the DRSOI, and (ii) the site-controlled growth mode of nanowires [24].

TABLE I. Fit parameters for the leakage current induced by the SOI. Γ describes the tunneling rate of $S(0,2)$ to the drain lead. $\gamma = \Gamma_{\mathrm{rel}}/\Gamma$, here Γ_{rel} describes the rate of relaxation from excited states to the ground state. t describes the tunnel coupling between the dots, and t_{SO} describes the coupling between the triplet $T(1,1)$ and singlet $S(0,2)$. I_0 is the background current. We can extract the spin-orbit length, l_{SO}, from the relationship $t_{\mathrm{SO}}/t = (4/3)(l_{\mathrm{dot}}/l_{\mathrm{SO}})$.

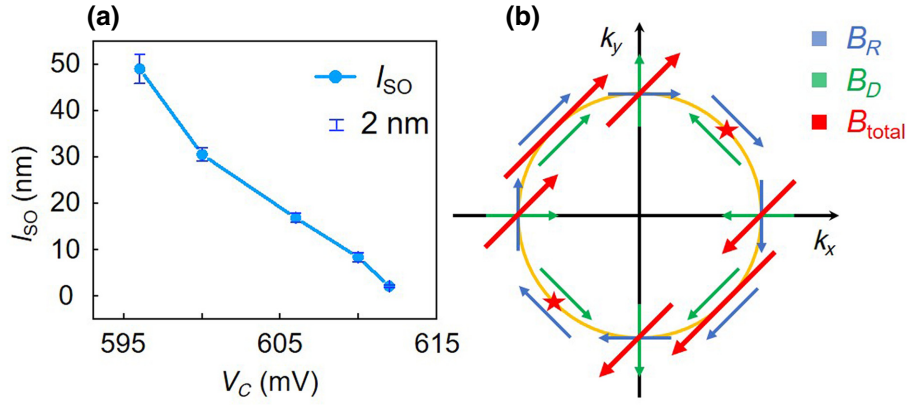| Data			Assumed parameter	Fitted parameters					Calculation
V_C (mV)	V_L (mV)	V_R (mV)	ξ	Γ (MHz)	γ	t (μeV)	t_{SO}(μeV)	I_0 (pA)	l_{SO}(nm)
596	510	516	0.14	1320 ± 20	0.008 ± 0.001	11.5 ± 0.5	23.5 ± 0.5	0.25 ± 0.05	48.9 ± 3.2
600	501	500	0.14	510 ± 5	0.02 ± 0.003	6 ± 0.2	19.7 ± 0.3	0.05 ± 0.05	30.5 ± 1.5
606	501	494	0.14	335 ± 5	0.055 ± 0.003	2.6 ± 0.1	15.5 ± 0.3	0.4 ± 0.05	16.8 ± 1.0
610	502	490	0.14	235 ± 5	0.075 ± 0.003	1.2 ± 0.1	14.5 ± 0.5	0.35 ± 0.05	8.3 ± 1.0
612	499	483	0.14	38 ± 1	2.1 ± 0.3	0.4 ± 0.05	20 ± 1	0.25 ± 0.03	2.0 ± 0.4

FIG. 4. (a) Spin-orbit length as a function of gate-C voltage, as extracted from fits to line cuts in Fig. 3(e). Error bars represent the calculation error of l_{SO}, which are determined by the fitting errors of parameters t and t_{SO} at difference V_C. (b) In momentum space, the effective spin-orbit fields are denoted by arrows of different colors: blue, direct Rashba SOI field (B_R); green, Dresshaus SOI field (B_D); red, total SOI field (B_{total}). B_R and B_D are equal in amplitude, and the total spin-orbit field will be completely turned off at the points marked by the red star.

Our results are obtained in the few-hole regime, though we expect that the SOI strength should remain highly tunable in quantum dots in the single-hole regime, as theoretical studies of DRSOIs [22,23] and other forms of SOI [33–35] were all done for single-hole quantum dots and did not require the presence of extra electrons or holes. In the meantime, applications in quantum-information processing may even be easier in the multihole regime [1–3,19], as explored before for multielectron spin qubits both theoretically and experimentally [56–59]. As such, our study of tunable SOIs should be relevant in a variety of situations.

III. CONCLUSION

We demonstrate experimentally a strongly tunable spin-orbit interaction in a lithographically defined DQD in a Ge hut wire that exhibits excellent charge stability. The multigate architecture provides independent control of the electron number in each dot as well as a highly tunable tunnel coupling from 0.4 to 11.5 μeV. By studying the magnetic field dependence of the leakage current in the PSB regime, we identify the SOI as the dominant spin-relaxation mechanism in our system. With increasing tunnel coupling, we observe a transition in the leakage current from a single peak at zero field to two peaks at finite magnetic fields induced through the effect of the SOI. Numerical calculations yield quantitative agreement with experimental results, showing a strong and tunable SOI with a spin-orbit length of $l_{SO} = 2.0$–48.9 nm in our system. These results provide promising evidence for potential spin-orbit switches and high-fidelity qubits in Ge HW QDs.

APPENDIX: MEASUREMENT DETAILS

Figure 5(a) shows the network of capacitors and voltage nodes that are used to calculate the conversion factors between the gate voltages and energy. Here, we consider the cross-talk between gate $L(R)$ and dot $R(L)$, and the four α_{il} values describe the coupling of gate i to the energy offset of the respective dot l. Figure 5(b) shows a charge-stability diagram over a wider range of gate sweeping compared to the one in Fig. 1(b). Notice the irregular distance between current peaks here, which is an indication that the addition energy includes both Coulomb interactions and single-particle excitation, and the system is in the few-hole regime. The gradient [k in Fig. 5(b)] of the charge transition (fit in yellow) yields the relative effect of the two gates on the single-particle energy offset of the same dot:

$$k_R = \frac{\delta V_L}{\delta V_R} = -\frac{\alpha_{RR}}{\alpha_{LR}} = -13, \tag{A1}$$

$$k_L = \frac{\delta V_L}{\delta V_R} = -\frac{\alpha_{RL}}{\alpha_{LL}} = -\frac{1}{22}. \tag{A2}$$

Figure 5(c) shows the bias triangle with a source-drain voltage of $V_{SD} = +2.5$ mV at a magnetic field of 50 mT.
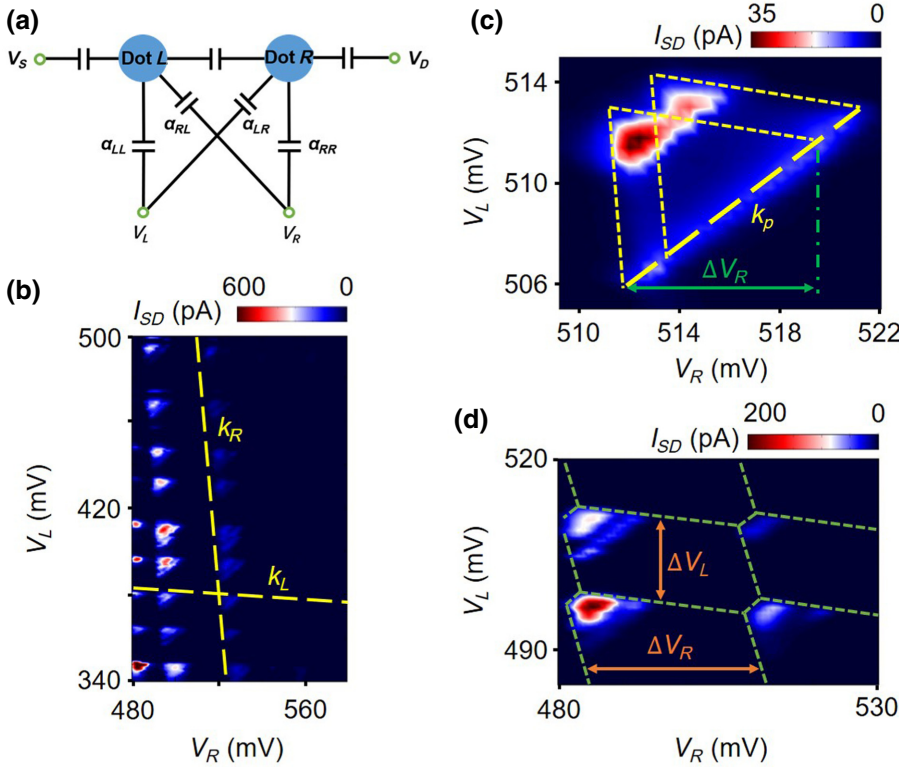
(a)

(b)

(c)

(d)

FIG. 5. (a) Network of capacitors and voltage nodes that are used to calculate the level arm. (b) Charge-stability diagram of the DQD over a wide range of gate voltages. Yellow dashed lines denote the charge-addition lines of two dots. (c) Bias triangle with a source-drain voltage of $V_{SD} = +2.5$ mV at a magnetic field of 50 mT. k_p is the gradient of the baseline of the triangle. (d) Same charge-stability diagram as that shown in Fig. 1(b). ΔV_i is the spacing of the charge-addition line of dot i.

As the difference between the single-particle energies of two dots stays fixed along a polarization line (the base of the triangle), we can determine the relative weights of the α_{il} values from the gradient (k_p) of this line in Fig. 5(c):

$$\alpha_{RR}\delta V_R + \alpha_{LR}\,\delta V_L = \alpha_{LL}\delta V_L + \alpha_{RL}\delta V_R, \qquad \text{(A3)}$$

$$k_p = \frac{\delta V_L}{\delta V_R} = 0.77. \qquad \text{(A4)}$$

At last, the absolute value of α_{il}, which is also called the lever arm, can be found from the length of the base of the triangle:

$$\alpha_{RR}\Delta V_R + \alpha_{LR}k_p\Delta V_R = eV_{SD} = 2.5 \text{ meV}. \qquad \text{(A5)}$$

Here, ΔV_R denotes the voltage change of gate R in the range of the bias triangle. Using Eqs. (A1)–(A5), we can extract the four values of the lever arms between the gate voltages and the energy of the dot: $\alpha_{LL} = 384.1$ meV V^{-1}, $\alpha_{LR} = 22.7$ meV V^{-1}, $\alpha_{RR} = 295$ meV V^{-1}, and $\alpha_{RL} = 17.5$ meV V^{-1}. Then, we can obtain the charging energies of two dots from the spacing of the charge-addition lines, as shown in Fig. 5(d): $E_C^R = \alpha_{RR}\Delta V_R = 8.6$ meV and $E_C^L = \alpha_{LL}\Delta V_L = 5.2$ meV.

[1] H. Watzinger, J. Kukučka, L. Vukušić, F. Gao, T. Wang, F. Schäffler, J.-J. Zhang, and G. Katsaros, A germanium hole spin qubit, Nat. Commun. **9**, 3902 (2018).

[2] F. N. M. Froning, L. C. Camenzind, O. A. H. van der Molen, A. Li, E. P. A. M. Bakkers, D. M. Zumbühl, and F. R. Braakman, Ultrafast hole spin qubit with gate-tunable spin-orbit switch, Nat Nanotechnol. **16**, 308 (2021).

[3] K. Wang, G. Xu, F. Gao, H. Liu, R. L. Ma, X. Zhang, Z. N. Wang, G. Cao, T. Wang, J.-J. Zhang, D. Culcer, X. D. Hu, H. W. Jiang, H. O. Li, G. C. Guo, and G. P. Guo, Ultrafast coherent of a hole spin qubit in a germanium quantum dot, Nat. Commun. **13**, 206 (2022).

[4] D. Jirovec, A. Hofmann, A. Ballabio, P. M. Mutter, G. Tavani, M. Botifoll, A. Crippa, J. Kukucka, O. Sagi, F. Martins, J. Saez-Mollejo, I. Prieto, M. Borovkov, J. Arbiol, D. Chrastina, G. Isella, and G. Katsaros, A singlet-triplet hole spin qubit in planar Ge, Nat. Mater. **20**, 1106 (2021).

[5] N. W. Hendrickx, W. I. L. Lawrie, L. Petit, A. Sammak, G. Scappucci, and M. Veldhorst, A single-hole spin qubit, Nat. Commun. **11**, 3478 (2020).

[6] N. W. Hendrickx, D. P. Franke, A. Sammak, G. Scappucci, and M. Veldhorst, Fast two-qubit logic with holes in germanium, Nature **577**, 487 (2020).

[7] N. W. Hendrickx, W. I. L. Lawrie, M. Russ, F. van Riggelen, S. L. de Snoo, R. N. Schouten, A. Sammak, G. Scappucci, and M. Veldhorst, A four-qubit germanium quantum processor, Nature **591**, 580 (2021).

[8] G. Scappucci, C. Kloeffel, F. A. Zwanenburg, D. Loss, M. Myronov, J.-J. Zhang, S. De Franceschi, G. Katsaros, and M. Veldhorst, The germanium quantum information route, Nat. Rev. Mater. **6**, 926 (2021).

[9] M. Veldhorst, J. C. C. Hwang, C. H. Yang, A. W. Leenstra, B. de Ronde, J. P. Dehollain, J. T. Muhonen, F. E. Hudson, K. M. Itoh, A. Morello, and A. S. Dzurak, An addressable quantum dot qubit with fault-tolerant control-fidelity, Nat. Nanotechnol. **9**, 981 (2014).

[10] X. Zhang, H.-O. Li, G. Cao, M. Xiao, G.-C. Guo, and G.-P. Guo, Semiconductor quantum computation, Nat. Sci. Rev. **6**, 32 (2019).

[11] P. Philippopoulos, S. Chesi, and W. A. Coish, First-principles hyperfine tensors for electrons and holes in GaAs and silicon, Phys. Rev. B **101**, 115302 (2020).

[12] J. Fischer, W. A. Coish, D. V. Bulaev, and D. Loss, Spin decoherence of a heavy hole coupled to nuclear spins in a quantum dot, Phys. Rev. B **78**, 155329 (2008).

[13] X. J. Wang, S. Chesi, and W. A. Coish, Spin-Echo Dynamics of a Heavy Hole in a Quantum Dot, Phys. Rev. Lett. **109**, 237601 (2012).

[14] S. Chesi, X. J. Wang, and W. A. Coish, Controlling hole spins in quantum dots and wells, Eur. Phys. J. Plus **129**, 86 (2014).

[15] X. J. Wang, S. Chesi, and W. A. Coish, Maximizing the purity of a qubit evolving in an anisotropic environment, Phys. Rev. B **92**, 115424 (2015).

[16] J.-W. Luo, S.-S. Li, and A. Zunger, Rapid Transition of the Hole Rashba Effect From Strong Field Dependence to Saturation in Semiconductor Nanowires, Phys. Rev. Lett. **119**, 126401 (2017).

[17] D. V. Bulaev and D. Loss, Electric Dipole Spin Resonance for Heavy Holes in Quantum Dots, Phys. Rev. Lett. **98**, 097202 (2007).

[18] V. S. Pribiag, S. Nadj-Perge, S. M. Frolov, J. W. G. van den Berg, I. van Weperen, S. R. Plissard, E. P. A. M. Bakkers, and L. P. Kouwenhoven, Electrical control of single hole spins in nanowire quantum dots, Nat. Nanotechnol. **8**, 170 (2013).

[19] R. Maurand, X. Jehl, D. Kotekar-Patil, A. Corna, H. Bohuslavskyi, R. Laviéville, L. Hutin, S. Barraud, M. Vinet, M. Sanquer, and S. De Franceschi, A CMOS silicon spin qubit, Nat. Commun. **7**, 13575 (2016).

[20] R. Li, J. Q. You, C. P. Sun, and F. Nori, Controlling a Nanowire Spin-Orbit Qubit via Electric-Dipole Spin Resonance, Phys. Rev. Lett. **111**, 086805 (2013).

[21] J.-J. Zhang, G. Katsaros, F. Montalenti, D. Scopece, R. O. Rezaev, C. Mickel, B. Rellinghaus, L. Miglio, S. De Franceschi, A. Rastelli, and O. G. Schmidt, Monolithic Growth of Ultrathin Ge Nanowires on Si(001), Phys. Rev. Lett. **109**, 085502 (2012).

[22] C. Kloeffel, M. Trif, and D. Loss, Strong spin-orbit interaction and helical hole states in Ge/Si nanowires, Phys. Rev. B **84**, 195314 (2011).

[23] C. Kloeffel, M. J. Rančić, and D. Loss, Direct Rashba spin-orbit interaction in Si and Ge nanowires with different growth directions, Phys. Rev. B **97**, 235422 (2018).

[24] F. Gao, J.-H. Wang, H. Watzinger, H. Hu, M. J. Rančić, J.-Y. Zhang, T. Wang, Y. Yao, G.-L. Wang, J. Kukučka, L. Vukušić, C. Kloeffel, D. Loss, F. Liu, G. Katsaros, and J.-J. Zhang, Site-controlled uniform Ge/Si hut wires with electrically tunable spin–orbit coupling, Adv. Mater. **32**, 1906523 (2020).

[25] Y. Hu, F. Kuemmeth, C. M. Lieber, and C. M. Marcus, Hole spin relaxation in Ge–Si core–shell nanowire qubits, Nat. Nanotechnol. **7**, 47 (2012).

[26] A. P. Higginbotham, T. W. Larsen, J. Yao, H. Yan, C. M. Lieber, C. M. Marcus, and F. Kuemmeth, Hole spin coherence in a Ge/Si heterostructure nanowire, Nano Lett. **14**, 3582 (2014).

[27] L. Vukušić, J. Kukučka, H. Watzinger, J. M. Milem, F. Schäffler, and G. Katsaros, Single-shot readout of hole spins in Ge, Nano Lett. **18**, 7141 (2018).

[28] A. V. Khaetskii and Yu. V. Nazarov, Spin-flip transitions between Zeeman sublevels in semiconductor quantum dots, Phys. Rev. B **64**, 125316 (2001).

[29] V. N. Golovach, A. V. Khaetskii, and D. Loss, Phonon-Induced Decay of the Electron Spin in Quantum Dots, Phys. Rev. Lett. **93**, 016601 (2004).

[30] P. Stano and J. Fabian, Theory of Phonon-Induced Spin Relaxation in Laterally Coupled Quantum Dots, Phys. Rev. Lett. **96**, 186602 (2006).

[31] R. Hanson, L. P. Kouwenhoven, J. R. Petta, S. Tarucha, and L. M. K. Vandersypen, Spins in few-electron quantum dots, Rev. Mod. Phys. **79**, 1217 (2007).

[32] F. Maier, C. Kloeffel, and D. Loss, Tunable g factor and phonon-mediated hole spin relaxation in Ge/Si nanowire quantum dots, Phys. Rev. B **87**, 161305 (2013).

[33] C. Kloeffel, M. Trif, P. Stano, and D. Loss, Circuit QED with hole-spin qubits in Ge/Si nanowire quantum dots, Phys. Rev. B **88**, 241405 (2013).

[34] S. Bosco, B. Hetényi, and D. Loss, Hole spin qubits in Si FinFETs with fully tunable spin-orbit coupling and sweet spots for charge noise, PRX Quantum **2**, 010348 (2021).

[35] T. Zhang, H. Liu, F. Gao, G. Xu, K. Wang, X. Zhang, G. Cao, T. Wang, J.-J. Zhang, X. Hu, H.-O. Li, and G.-P. Guo, Anisotropic *g*-factor and spin–orbit field in a germanium hut wire double quantum dot, Nano Lett. **21**, 3835 (2021).

[36] A. Zarassi, Z. Su, J. Danon, J. Schwenderling, M. Hocevar, B. M. Nguyen, J. Yoo, S. A. Dayeh, and S. M. Frolov, Magnetic field evolution of spin blockade in Ge/Si nanowire double quantum dots, Phys. Rev. B **95**, 155416 (2017).

[37] K. Ono, D. G. Austing, Y. Tokura, and S. Tarucha, Current rectification by pauli exclusion in a weakly coupled double quantum dot system, Science **297**, 1313 (2002).

[38] K. Ono, G. Giavaras, T. Tanamoto, T. Ohguro, X. Hu, and F. Nori, Hole Spin Resonance and Spin-Orbit Coupling in a Silicon Metal-Oxide-Semiconductor Field-Effect Transistor, Phys. Rev. Lett. **119**, 156802 (2017).

[39] K. Ono, S. N. Shevchenko, T. Mori, S. Moriyama, and F. Nori, Quantum Interferometry With a *g*-Factor-Tunable Spin Qubit, Phys. Rev. Lett. **122**, 207703 (2019).

[40] G. Xu, F. Gao, K. Wang, T. Zhang, H. Liu, G. Cao, T. Wang, J.-J. Zhang, H. W. Jiang, H. O. Li, and G.-P. Guo, Hole spin in tunable Ge hut wire double quantum dot, Appl. Phys. Express. **13**, 065002 (2020).

[41] J. Danon and Yu. V. Nazarov, Pauli spin blockade in the presence of strong spin-orbit coupling, Phys. Rev. B **80**, 041301 (2009).

[42] F. H. L. Koppens, J. A. Folk, J. M. Elzerman, R. Hanson, L. H. W. van Beveren, I. T. Vink, H. P. Trantiz, W. Wegscheider, L. P. Kouwenhoven, and L. M. K. Vandersypen, Control and detection of singlet-triplet mixing in a random nuclear field, Science **309**, 1346 (2005).

[43] O. N. Jouravlev and Y. V. Nazarov, Electron Transport in a Double Quantum Dot Governed by a Nuclear Magnetic Field, Phys. Rev. Lett. **96**, 176804 (2006).

[44] N. S. Lai, W. H. Lim, C. H. Yang, F. A. Zwanenburg, W. A. Coish, F. Qassemi, A. Morello, and A. S. Dzurak, Pauli

spin blockade in a highly tunable silicon double quantum dot, Sci. Rep. **1,** 110 (2011).

[45] M. Brauns, J. Ridderbos, A. Li, E. P. A. M. Bakkers, W. G. van der Wiel, and F. A. Zwanenburg, Anisotropic Pauli spin blockade in hole quantum dots, Phys. Rev. B **94,** 041411(R) (2016).

[46] F. Qassemi, W. A. Coish, and F. K. Wilhelm, Stationary and Transient Leakage Current in the Pauli Spin Blockade, Phys. Rev. Lett. **102,** 176806 (2009).

[47] W. A. Coish and F. Qassemi, Leakage-current line shapes from inelastic cotunneling in the Pauli spin blockade regime, Phys. Rev. B **84,** 245407 (2011).

[48] L. V. C. Assali, H. M. Petrilli, R. B. Capaz, B. Koiller, X. Hu, and S. Das Sarma, Hyperfine interactions in silicon quantum dots, Phys. Rev. B **83,** 165301 (2011).

[49] H. Watzinger, C. Kloeffel, L. Vukusic, M. D. Rossell, V. Sessi, J. Kukucka, R. Kirchschlager, E. Lausecker, A. Truhlar, M. Glaser, A. Rastelli, A. Fuhrer, D. Loss, and G. Katsaros, Heavy-hole states in germanium hut wires, Nano Lett. **16,** 6879 (2016).

[50] P. M. Mutter and G. Burkard, *g*-Tensor resonance in double quantum dots with site-dependent *g*-tensors, Mater. Quantum. Technol. **1,** 015003 (2020).

[51] N. Ares, V. N. Golovach, G. Katsaros, M. Stoffel, F. Fournel, L. I. Glazman, O. G. Schmidt, and S. De Franceschi, Nature of Tunable Hole g Factors in Quantum Dots, Phys. Rev. Lett. **110,** 046602 (2013).

[52] A. V. Nenashev, A. V. Dvurechenskii, and A. F. Zinovieva, Wave functions and g factor of holes in Ge/Si quantum dots, Phys. Rev. B **67,** 205301 (2003).

[53] S. Nadj-Perge, S. M. Frolov, J. W. W. van Tilburg, J. Danon, Yu. V. Nazarov, R. Algra, E. P. A. M. Bakkers, and L. P. Kouwenhoven, Disentangling the effects of spin-orbit and hyperfine interactions on spin blockade, Phys. Rev. B **81,** 201305 (2010).

[54] D. Stepanenko, M. Rudner, B. I. Halperin, and D. Loss, Singlet-triplet splitting in double quantum dots due to spin-orbit and hyperfine interactions, Phys. Rev. B **85,** 075416 (2012).

[55] K. Takeda, J. Kamioka, T. Otsuka, J. Yoneda, T. Nakajima, M. R. Delbecq, S. Amaha, G. Allison, T. Kodera, S. Oda, and S. Tarucha, A fault-tolerant addressable spin qubit in a natural silicon quantum dot, Sci. Adv. **2,** e1600694 (2016).

[56] X. Hu and S. Das Sarma, Spin-based quantum computation in multielectron quantum dots, Phys. Rev. A **64,** 042312 (2001).

[57] E. Barnes, J. P. Kestner, N. T. T. Nguyen, and S. Das Sarma, Screening of charged impurities with multielectron singlet-triplet spin qubits in quantum dots, Phys. Rev. B **84,** 235309 (2011).

[58] A. P. Higginbotham, F. Kuemmeth, M. P. Hanson, A. C. Gossard, and C. M. Marcus, Coherent Operations and Screening in Multielectron Spin Qubits, Phys. Rev. Lett. **112,** 026801 (2014).

[59] R. C. C. Leon, C. H. Yang, J. C. C. Hwang, J. Camirand Lemyre, T. Tanttu, W. Huang, K. W. Chan, K. Y. Tan, F. E. Hudson, K. M. Itoh, A. Morello, A. Laucht, M. Pioro-Ladrière, A. Saraiva, and A. S. Dzurak, Coherent spin control of s-, p-, d- and f-electrons in a silicon quantum dot, Nat. Commun. **11,** 797 (2020).

Correction: A proof change request to alter the last column heading in Table I was misinterpreted and has been set right.